

Reducing Stress Concentration in the Transition Region of Coilable Ultra-Thin-Shell Booms

Christophe Leclerc* and Sergio Pellegrino†
California Institute of Technology, Pasadena, CA, 91125

High stress concentrations leading to material failure have been observed in TRAC booms coiled under tension around a circular hub. The stress concentrations are typically observed in the transition region between the fully deployed and coiled sections of the boom. A numerical simulation framework is proposed to model the coiling process and analyse the stress distribution in the transition region. Isotropic booms are first studied to understand the effects of the cross-section geometry and the boundary conditions during coiling. Compressive stress is reduced by 13% and 26% by using a variable curvature cross-section and adding nip rollers in the coiling mechanism respectively. For an ultra-thin glass fiber-carbon fiber composite laminate, the compressive stress is similarly reduced by 24% and 11%. The variable curvature cross-section is shown to eliminate the stress concentration in the transition region.

Nomenclature

F	Tension force
R_N	Nip rollers radius
R	Hub radius
X, Y, Z	Global coordinate system
d_N	Distance between nip rollers and hub
r	Flange radius of curvature
t	Flange thickness
w	Web width
x, y, z	Local shell coordinate system
$\Delta\kappa_x$	Change of curvature in the longitudinal direction
$\Delta\kappa_y$	Change of curvature in the transverse direction
θ	Flange opening angle
σ_{xx}	Normal stress in the longitudinal direction
σ_{yy}	Normal stress in the transverse direction

I. Introduction

Coilable booms, such as the Storable Tubular Extendable Member (STEM) and the Collapsible Tube Mast (CTM) have been used extensively in spacecraft structures due to their efficient packaging and simple deployment. A more recent design, the Triangular Rollable And Collapsible (TRAC) boom, was developed by the Air Force Research Laboratory [1]. The TRAC boom consists of two circular arc flanges joined at a flat web, flattened and coiled around a circular hub as shown in Figure 1. In one packaging concept, a mechanism can be used to apply tension F at the tip of the boom while driving a rotating hub at angular velocity ω , also shown in Figure 1. The TRAC boom has been integrated in multiple spacecraft designs [2, 3], and flown on two different solar sail missions, NASA's NanoSail-D [4, 5] and the Planetary Society's LightSail-A [6].

TRAC booms made of composite materials have been studied extensively in recent years. The mechanical properties in the deployed configuration, such as the bending stiffness and the buckling load, have been well characterized using a combination of analytical formulations, numerical simulations and experimental work [7–10]. Recent research has

*Graduate Student, Graduate Aerospace Laboratories, 1200 E California Blvd. MC 205-45. AIAA Student Member. e-mail: cleclerc@caltech.edu

†Joyce and Kent Kresa Professor of Aerospace and Civil Engineering, Graduate Aerospace Laboratories, 1200 E California Blvd. MC 105-50. AIAA Fellow. e-mail: sergiop@caltech.edu

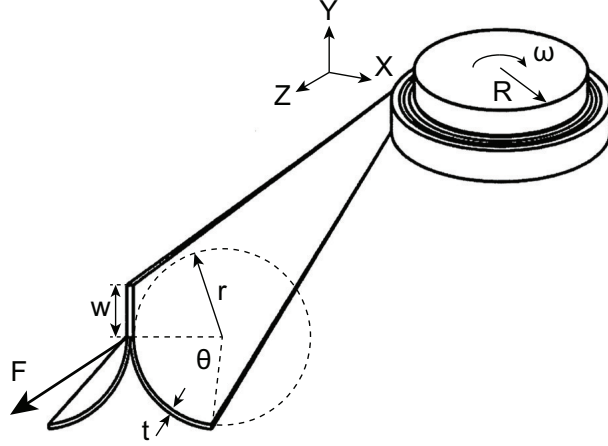


Fig. 1 Schematic of tension-stabilized TRAC boom (modified from Banik and Murphey [7]).

shown that using ultra-thin composites in TRAC booms can reduce significantly the packaged volume, extending the range of applications. However, greatly decreasing the thickness of the booms has brought up new issues specific to ultra-thin shells, such as inner flange buckling and blossoming of the coiled region of the booms, both having a negative impact on packaging efficiency and deployment [8, 11, 12]. The application of a longitudinal tension to the booms has been shown to help reduce instabilities and prevent blossoming. This allowed the booms to be wrapped around cylinders with smaller radii, also enabling packaging of long structures, where the coiling radius significantly increases as the boom wraps over itself multiple times. It has also been observed that high stress concentration, leading to material failure, occurs in the transition region from the fully deployed configuration to the fully coiled configuration. As the coiling was done at a constant, low velocity, the transition region was in a steady state and hence inertia plays no role [13].

The minimum achievable coiling radius has been studied for a wide range of composite laminates [7, 11]. However, those limits were obtained without taking into consideration the stress concentrations in the transition region described above. When studying the effect of the transition region, previous research has shown that changing the composite laminate for a TRAC boom from a 4-ply $[0/90]_S$ carbon fiber prepreg laminate to a 3-ply $[0/90/0]$, keeping everything else constant, decreased peak stresses by 21% [13].

The present work aims at reducing the minimum radius around which a coilable boom can be packaged without failure, enabling more efficient packaging. The effect of varying three design parameters is studied: boom material, cross-section geometry, and boundary conditions during coiling. In order to decouple these three parameters, booms made of isotropic materials are studied first. The paper is presented in four sections. First, a simulation framework to compare different designs is presented, enabling comparison of different designs. Next, structures made of isotropic material are studied analytically and using numerical simulations. Then, booms made of orthotropic material are investigated. The final section summarizes and discusses the key findings.

II. Numerical Simulation Framework

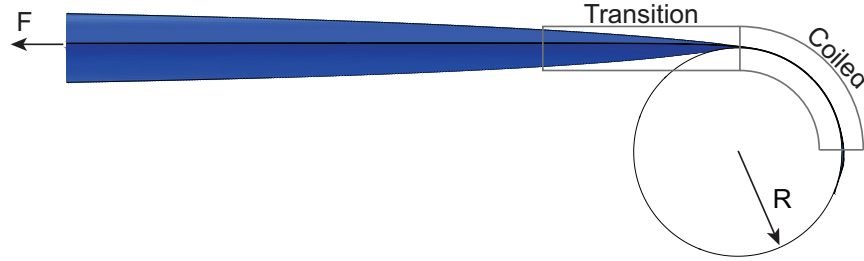
Designing a coilable boom requires a method to quickly assess different designs and extract meaningful results for comparison. A numerical simulation framework was therefore developed using the commercial finite element software Simulia ABAQUS Standard 2016. The problem consists of three pieces: a shell structure, defined by geometric and mechanical parameters; a coiling mechanism (hub), defined by R ; a tension force F applied axially. The boom is 550 mm long and is modeled using reduced integration four-node quadrilateral thin-shell elements. It is composed of an inner flange (in contact with the hub) and an outer flange, bonded together using tie constraints along the web. A rigid clamp flattens the end of the structure and holds it against the hub. The full model is shown in Figure 2a.

The simulation consists of the three following steps:

- 1) The boom is flattened at one end by moving the clamp and the hub towards each other;
- 2) An axial load is applied at the other end of the boom;
- 3) The boom is coiled around the hub by imposing an angular velocity to the hub and the clamp.



(a) Initial configuration of the model.



(b) Coiled model under tension with regions of interest.

Fig. 2 Finite element model of the coilable boom.

The coiled model is shown in Figure 2b, with the two regions of interest, transition and fully coiled, marked. For the current study, $F = 15 \text{ N}$ and $R = 25.4 \text{ mm}$ are kept constant to match previous work [13].

The axial load is added to stabilize the boom during coiling. Two different types of contacts are defined in the simulation to prescribe interactions between the different parts. During flattening, frictionless contact is defined between the two flanges, the hub and the clamp. Once flattening has been achieved, the contact formulation between the top flange and the clamp is changed to prevent any tangential relative movement ("rough" friction formulation), allowing the coiling of the boom to be driven by the clamp rotation with the hub. At the other end of the boom, the axial load is applied at a reference point kinematically constrained to all the end nodes. During the second step, additional constraints are temporarily applied at the nodes of the web, preventing any displacement other than along the axis of the boom. This stabilizes the boom helping quick convergence during that step. These constraints are removed prior to the third step.

The simulation uses a quasi-static dynamic implicit formulation, a trade-off between static implicit and explicit approaches. It converges to a final static response by using implicit time integration where inertia effects are introduced to help convergence of unstable behavior, for example due to nonlinearities and contacts. Numerical damping is introduced at each time step to reach convergence. A mesh convergence study showed that 40 elements across the flange arc-length were sufficient to fully capture highly localized effects.

III. Isotropic Booms

Previous research on ultra-thin composite TRAC booms has shown a significant stress concentration in the transition region between the fully coiled and the fully deployed configuration [13]. However, it was unclear if the high stress was due to (i) the orthotropic material, (ii) the cross-section geometry, (iii) the coiling process, or a combination of these effects. In order to study the second and third effects, the present section studies a coilable boom made of isotropic material.

As the behavior during coiling is mainly driven by the shell bending stiffness, the material properties for the isotropic boom were chosen to match the bending stiffness of the orthotropic laminate selected in Section IV, using the equation:

$$\left(\frac{Et^3}{12(1-\nu^2)} \right)_{iso} = (D_{11})_{ortho} \quad (1)$$

where the left-hand side is the plate flexural rigidity of the isotropic material, and D_{11} is the first element of the composite material bending matrix, obtained using the Classical Lamination Theory. Assuming for the isotropic material $E = 69$ GPa and $\nu = 0.33$, this results in a flange thickness of $60 \mu\text{m}$.

Three different structures are analyzed in this section. The first one is a reference geometry chosen to provide benchmark results to which other designs can be compared. The second structure has an variable curvature cross-section in order to reduce the maximum stress. The last structure uses the same cross-section as the reference, but the coiling process is modified by creating a two-step transition region, again to reduce the maximum stress. For each case, a coiling simulation is performed and the stresses in the inner flange are extracted. Stresses in the outer flange are consistently much smaller and therefore are not included in the paper.

Stresses from the simulation are extracted at three different integration points across the thickness for each flange, and are expressed in the local shell coordinate system, as shown in Figure 3.

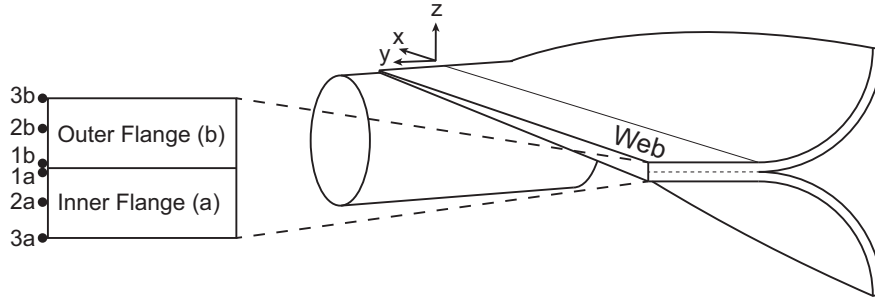


Fig. 3 Numbering convention for the integration points, and local shell coordinate system definition.

A. Reference Cross-Section

A baseline coilable structure design is chosen to match previous work [13]. It is a TRAC boom with the following dimensions: $r = 10.6$ mm, $\theta = 105^\circ$ and $w = 8$ mm. Simple estimates of the stresses in the fully coiled region in the inner flange can be obtained using the following equations:

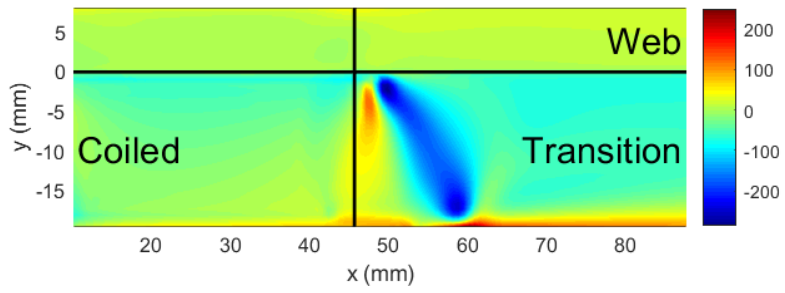
$$\Delta\kappa_x = \frac{1}{R} \quad \text{and} \quad \Delta\kappa_y = \frac{1}{r} \quad (2)$$

$$\sigma_{xx,max} = E \cdot \epsilon_{xx,max} = \Delta\kappa_x \cdot Et = -\frac{Et}{R} \quad (3)$$

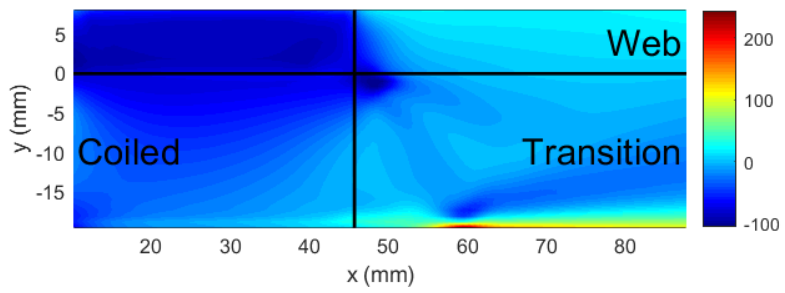
$$\sigma_{yy,max} = E \cdot \epsilon_{yy,max} = \pm\Delta\kappa_y \cdot E \frac{t}{2} = \pm\frac{Et}{2r} \quad (4)$$

In the flanges, the radius of curvature changes from 0 to R in x , and from r to 0 in y . The web only has the curvature change in x . The equation for the longitudinal stress σ_{xx} assumes that the two flanges are coiled together without relative shear displacement, which is true in the web. Therefore, the strain is always compressive in the inner flange, and goes from a maximum on the surface in contact with the hub (equation 3), to zero on the surface in contact with the outer flange. The transverse stress goes from a maximum tensile value on the inner surface of the inner flange, to a maximum compressive value on the outer surface of the inner flange. Using the aforementioned isotropic material properties, the maximum estimated stresses in the fully coiled region are $\sigma_{xx,max} = -160$ MPa and $\sigma_{yy,max} = \pm 200$ MPa.

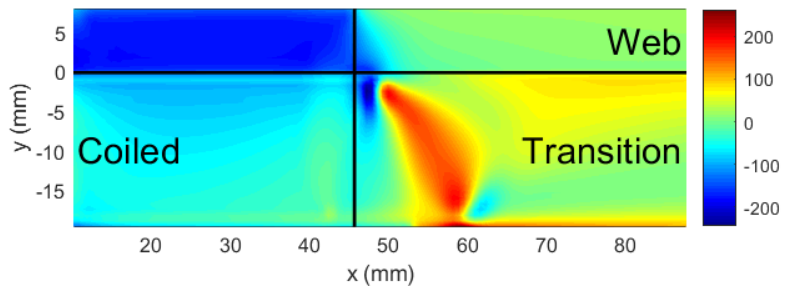
The stress results from the simulation can be seen in Figures 4 and 5. The plots show the stress distribution in the inner flange unwrapped and projected onto a plane for the sake of clarity. The plots are centered around the location of contact between the boom and the hub, marked as a black vertical line. Only the stresses in a 8 cm long region of the boom are shown, because it encompasses both the fully coiled region and the transition region. Figure 4 displays the variation of the longitudinal stress (σ_{xx}) at the location of each integration point through the thickness, and Figure 5 presents similar results for the transverse stress (σ_{yy}).



(a) Integration point 1a

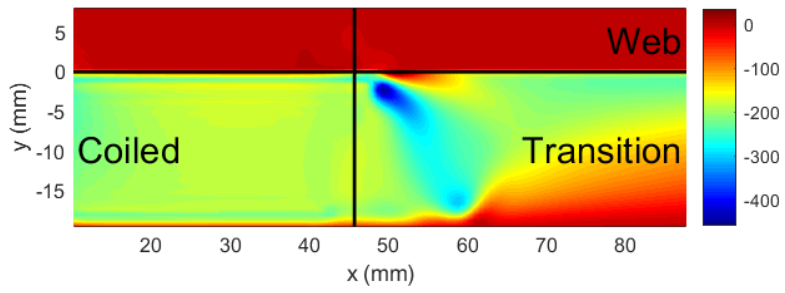


(b) Integration point 2a

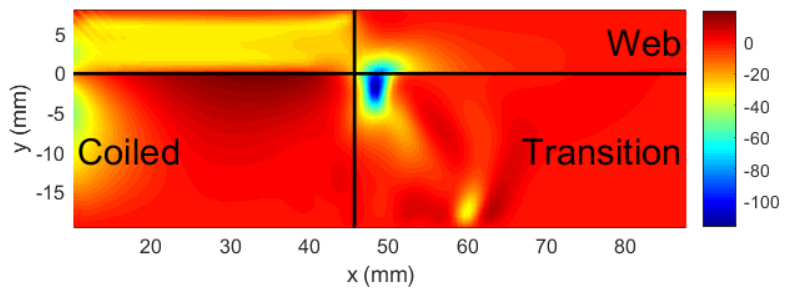


(c) Integration point 3a

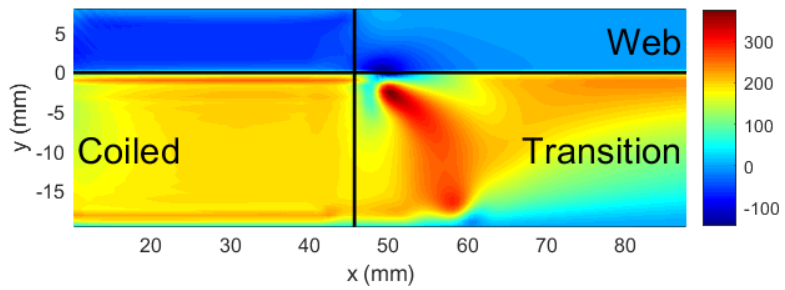
Fig. 4 σ_{xx} (MPa) in the inner flange of the reference isotropic structure.



(a) Integration point 1a



(b) Integration point 2a



(c) Integration point 3a

Fig. 5 σ_{yy} (MPa) in the inner flange of the reference isotropic structure.

These plots show a zone of high stress concentration that goes from the root of the web, where the inner flange is fully in contact with the hub, to the free edge of the flange further up in the transition region. The highest compressive stress (-460 MPa) is in the transverse direction, very close to both the web and the hub (integration point 1a, Figure 5a). The highest tensile stress (380 MPa) is also in the transverse direction and at a similar location, but at a different depth in the material (integration point 3a, Figure 5c).

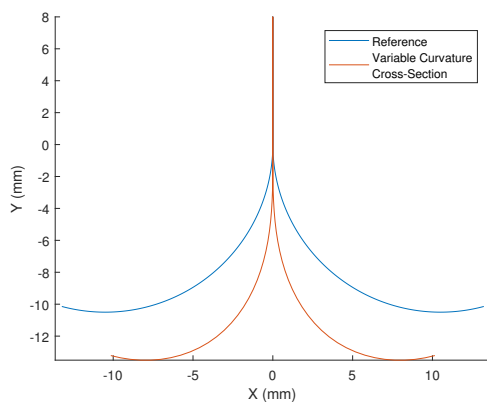
These results demonstrate that the current structure design and coiling mechanism lead to a very high stress concentration during coiling. Indeed, in the fully coiled region, the maximum compressive stress (-200 MPa) and tensile stress (200 MPa) are only 43% and 53% of their respective maximum values in the transition region. Furthermore, while the simple analytical equations predict accurately the stress in the transverse direction, they overestimate the stress in the longitudinal direction. Indeed, σ_{xx} in the coiled region from the simulation, at integration point 3a, varies from -40 MPa at the free edge to -100 MPa close to the web, compared to -160 MPa predicted by the equation. The longitudinal stress in the web is well predicted by the equations, going from zero at integration point 1a to -180 MPa at integration point 3a.

B. Variable Curvature Cross-Section

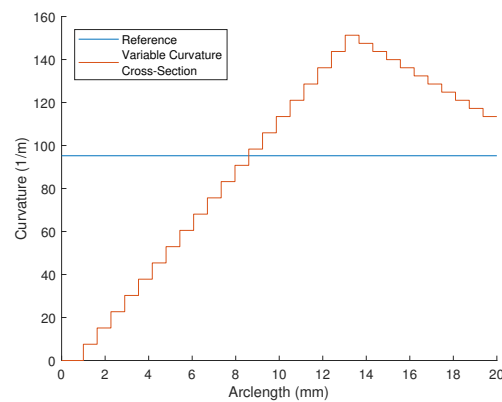
The previous section has shown that a high stress concentration occurs in the transition region of the reference structure. One possible reason behind this stress peak, and its location, is that the cross-section has a curvature discontinuity between the flange (constant radius) and the web (zero curvature). To avoid this discontinuity and reduce the stress concentration, a cross-section with smoothly varying curvature was analysed. While the web stays unchanged, a curvature profile is imposed to the flange. To reduce the design space, the total arc-length of the flange is kept constant, ensuring a constant amount of material between the different designs. Furthermore, to keep the comparison as fair as possible, the opening angle (defined as the angle between the web and the tangent of the flange at the free edge) is also kept constant at 105° .

To generate the cross-section, a curvature profile (continuous function) is discretized into 30 circular arcs with different radii. Then, a spline is used to smooth the profile, and the resulting cross-section is input into the simulation. A simple way to avoid the curvature discontinuity would be to linearly increase the curvature, starting with zero curvature at the web and reaching a maximum at the free edge. However, due to the two imposed constraints (arc-length and opening angle), this leads to a high curvature close to the edge of the flange, and thus high stress due to flattening. A better approach is to (i) initially increase the curvature, starting with zero curvature at the web, and then (ii) decrease it close to the edge. Multiple cross-sections were thus generated by changing the relative slopes between (i) and (ii), but only the cross-section leading to the lowest stresses is presented in this paper.

The chosen cross-section is shown in Figure 6a, while the discretized curvature profile is shown in Figure 6b. Due to the linearly varying curvature, there is now no discontinuity at the transition from the web to the flange.



(a) Comparison of the variable curvature cross section with the reference structure.



(b) Curvature profile of the variable curvature cross-section (excluding web region).

Fig. 6 Variable curvature cross-section.

The transverse stress (σ_{yy}) results from the simulation can be seen in Figure 7. Stresses in the longitudinal direction (σ_{xx}) are not included as the values are always smaller than in the transverse direction. These results show a reduction

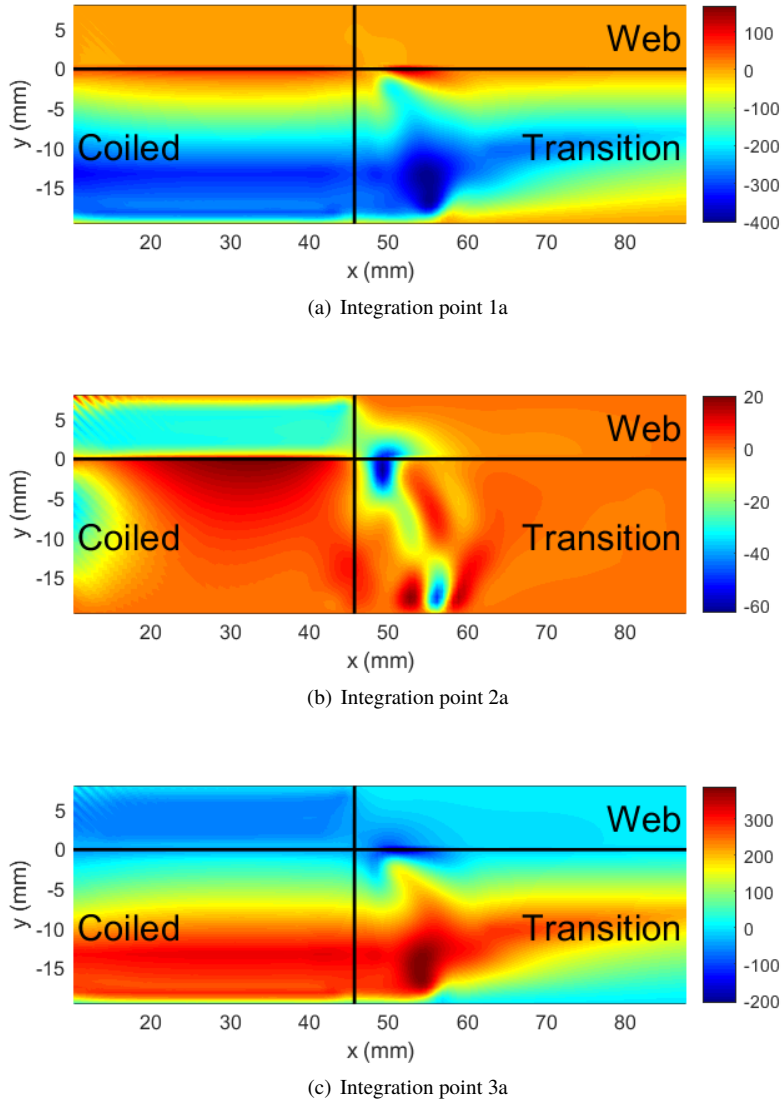
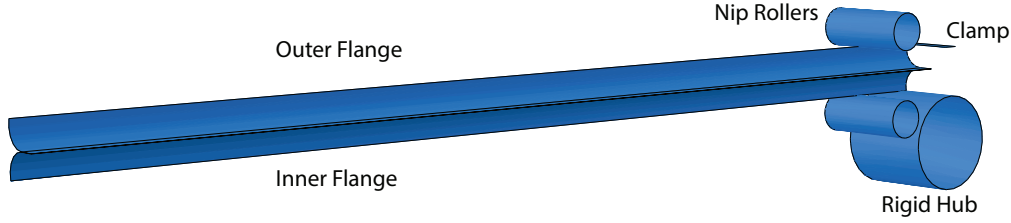


Fig. 7 σ_{yy} (MPa) in the inner flange of the isotropic structure with variable curvature cross-section.

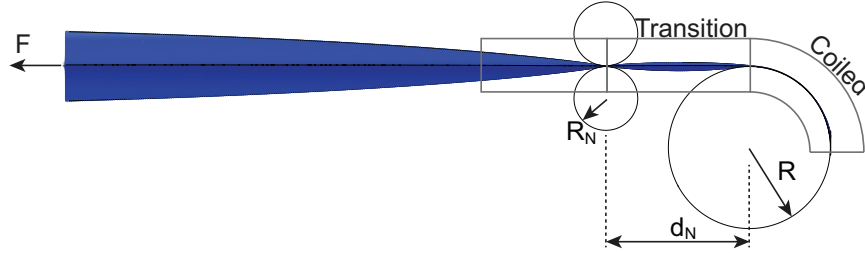
of the stress when compared with the reference structure. The maximum compressive stress is now -400 MPa (87% of the reference value), while the maximum tensile stress is similar to the reference value. Furthermore, the location of the peak stress has moved from the root of the web to the middle of the flange.

C. Two-Step Transition Region Coiling Process

In order for the structure to go from the fully deployed configuration to the packaged configuration, the flanges need to undergo two shape changes, as the curvature changes in two directions: flattening ($\Delta\kappa_y$) and coiling ($\Delta\kappa_x$). Using the current mechanism, as described in Section II, these two deformations occur simultaneously in a region close to the hub. This location also corresponds to the stress peak observed in the reference structure. In order to decouple the effects of flattening from coiling and better understand the influence of each of them on the stress distribution, a new coiling mechanism was considered, similar to winding machines [14]. Two nip rollers with radius R_N are added upstream of the hub at a center-to-center offset d_N , as shown in Figure 8. During the flattening step, the two rollers are moved closer together at the same time as the clamp and the hub, flattening the structure. The final gap between the two rollers is kept at 200 μm greater than the boom total thickness to help convergence of the simulation. During the coiling step,



(a) Initial configuration of the model.



(b) Coiled model under tension with regions of interest.

Fig. 8 Finite elements model of the coilable structure with the two-step transition region.

frictionless contact is imposed between the boom and the cylinders. This new mechanism therefore flattens the structure before it reaches the hub for coiling, decoupling the two deformations.

In order to obtain a comparison with the reference structure, a simulation was performed using the reference cross-section. The transverse stress (σ_{yy}) results for $R_N = 10$ mm and $d_N = 35$ mm can be seen in Figure 9. Once again, these results show a clear reduction of the stress when compared with the reference structure. The maximum compressive stress is now -340 MPa (74% of the reference value), while the maximum tensile stress is reduced to 310 MPa (82% of the reference value). Using this new mechanism, the maximum stresses are only 50% higher than their equivalent values in the fully coiled region. Finally, decreasing d_N to 25 mm increased slightly the maximum stresses to -360 MPa and 340 MPa, showing that the results are not very sensitive to d_N .

IV. Orthotropic Booms

While studying structures made of isotropic material helped better understand the effect of the geometry and the boundary conditions on the stress concentration during coiling, the end objective is to develop ultra-thin coilable structures made of composite material. Therefore, this section builds on the main findings of the previous section and applies them to the case of orthotropic structures.

A. Reference Cross-Section

The same reference cross-section as the isotropic structure is used here for the orthotropic case. Previous research [13] studied this type of structure using two different composite laminates made from thin-ply unidirectional carbon fiber tapes: $[0/90]_S$ (4-ply) and $[0/90/0]$ (3-ply). In both cases, the maximum stress is in the transverse direction (in a 90° ply), which is consistent with the results from the previous section.

Therefore, one solution to reduce the stress is to remove altogether the 90° plies, and add a layer of plain weave glass fiber fabric to give some in-plane shear and transverse strength to the laminate [15, 16]. As the mechanical properties of the deployed structure are mainly driven by the amount of 0° fibers, this new laminate has similar deployed properties. Furthermore, the glass fiber plain weave is tougher and has a higher strain limit. While multiple different laminates were studied, the results from only one laminate are presented here.

The new laminate is $[\pm 45_{GFPW}/0_{2CF}/\pm 45_{GFPW}]$, where $GFPW$ denotes a glass fiber plain weave prepreg made with JPS E-glass fabric (style 1067) and Patz PMT-F4 epoxy resin, and CF denotes a unidirectional carbon fiber prepreg tape made of Torayca T800 carbon fibers with NTPT ThinPreg 402 epoxy resin. Table 1 summarizes the elastic properties for these two materials.

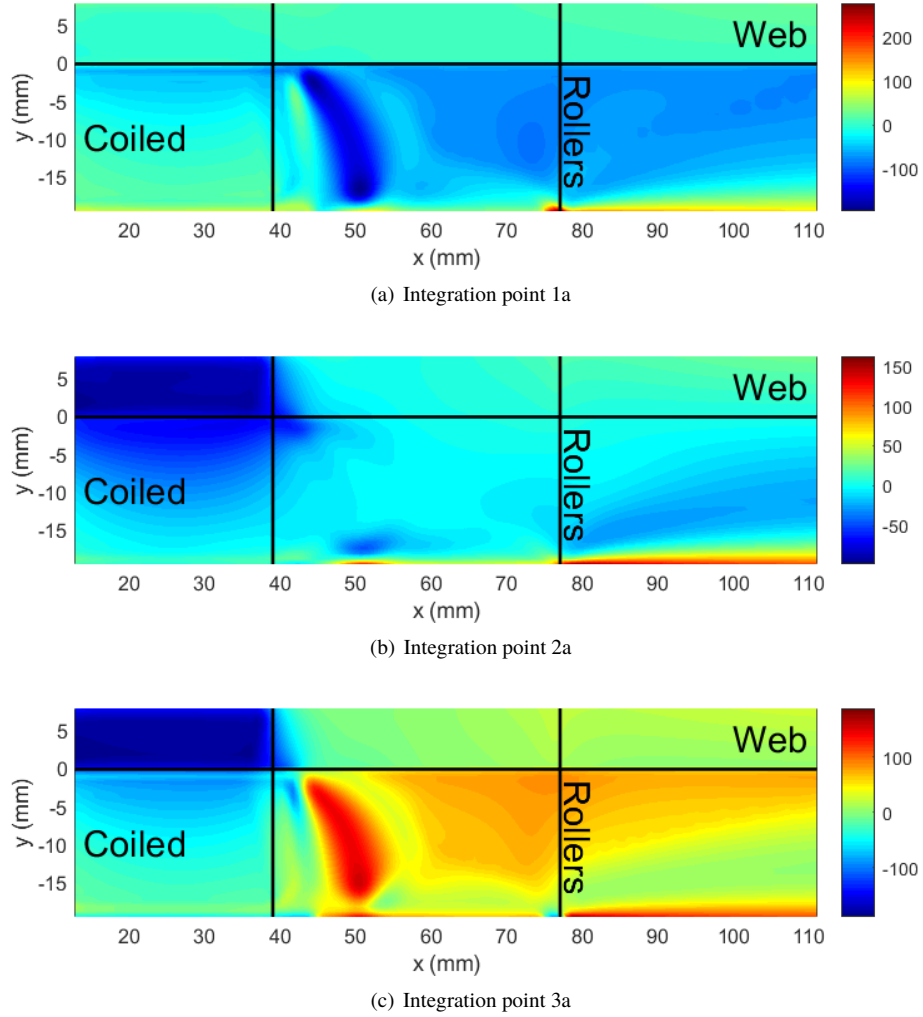


Fig. 9 σ_{yy} (MPa) in the inner flange of the isotropic structure with the two-step transition region.

Table 1 Elastic properties for the carbon fiber and glass fiber plain weave prepreg.

	E_1 [GPa]	E_2 [GPa]	G_{12} [GPa]	ν_{12}	t [μm]
CF	128	6.5	7.5	0.35	17.75
GFPW	24	24	3.3	0.17	25

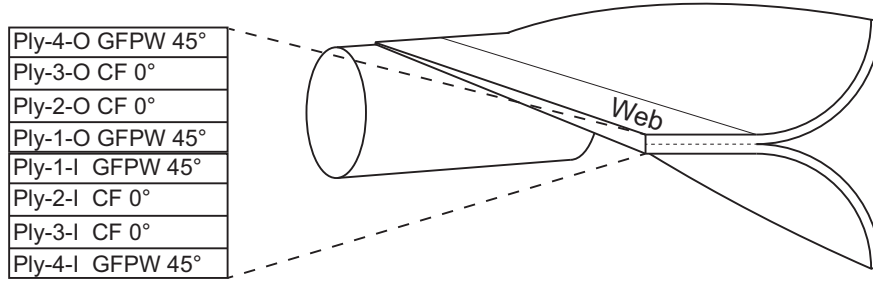


Fig. 10 Naming convention for the composite plies. *I* denotes inner flange, and *O* denotes outer flange.

This new laminate was investigated using the simulation framework presented in Section II. Now that each flange is composed of 4 plies, a modified numbering scheme for the integration points is used, as shown in Figure 10. For each ply, results are extracted at three integration points, where 3 is always the closest to the hub and 1 is the furthest. The longitudinal stresses obtained from the simulation are shown in Figures 11 (ply-2-I) and 12 (ply-3-I). Using this new laminate, the maximum compressive stress was found to be -460 MPa (ply-3-I, integration point 3, Figure 12c). The maximal tensile stress obtained was 330 MPa (ply-3-I, integration point 3, Figure 11a), located at the free edge of the flange.

For the remaining of the orthotropic boom study, the comparison will be done only with the maximum compressive stress in the carbon fiber plies, as the tensile stress is always smaller.

B. Variable Curvature Cross-Section

The maximum compressive stress observed in the orthotropic variable cross-section structure presented in Section III.B (-350 MPa) was 76% of the maximal stress observed in the reference structure (-460 MPa). This maximum stress occurs in ply-3-I, integration point 3, shown in Figure 13. Furthermore, the variable cross-section structure exhibits no compressive stress concentration in the transition region, with the maximum compressive stress located in the fully coiled region. All the variable curvature cross-sections generated for the isotropic boom were simulated with the composite laminate properties and the same cross-section (Figure 6) led to the minimum stresses.

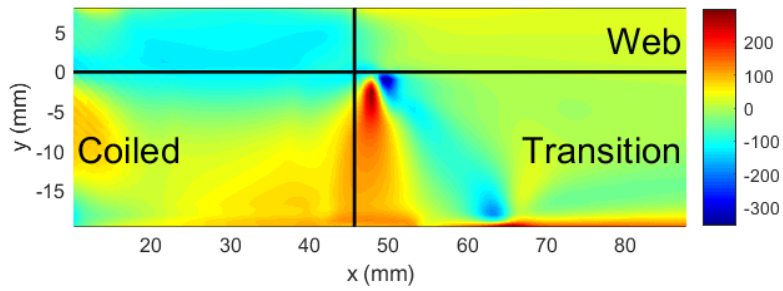
C. Two-Step Transition Region Coiling Process

The last study for the orthotropic boom used the modified two-step transition region presented in section III.C. The final gap between the two nip rollers was reduced to exactly the total thickness of the boom in order to achieve convergence during the simulation. The resulting longitudinal stress (for $R_N = 10$ mm and $d_N = 35$ mm) in ply-3-I, integration point 3, is shown in Figure 14, as this corresponds to the point of maximum compressive stress (-410 MPa). This is a reduction of 11% of the maximal stress obtained for the reference case (-460 MPa).

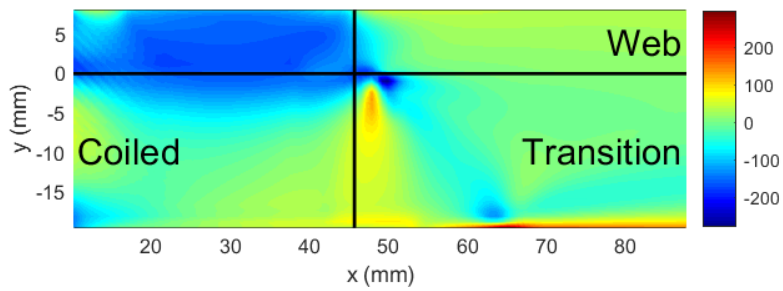
V. Discussion

While the TRAC boom compares very favorably with the STEM and the CTM in terms of bending stiffness to packaged height ratio [17], high stress concentrations have been observed during TRAC boom coiling. Previously, reduced hub radii and smaller laminate thicknesses were demonstrated to avoid material failure [13]. To enable tighter packaging, the maximum stress must be reduced. This study investigates the effect of a variable curvature cross-section, nip rollers in the coiling mechanism and isotropic material properties on the previously observed stress concentration, and the conjecture that the stress concentration is due to the TRAC geometry and the boundary conditions during coiling.

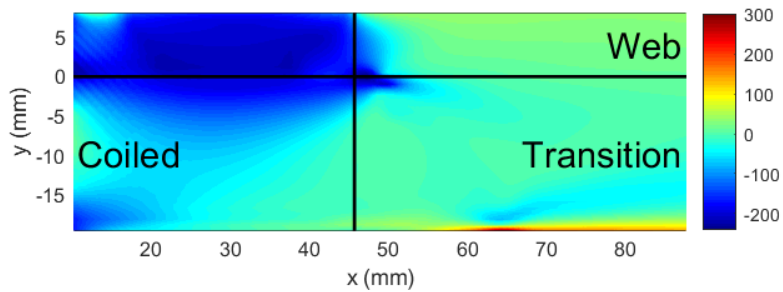
Comparing Figures 4c and 12c qualitatively, the longitudinal stress distributions in the transition region are similar for the isotropic and orthotropic booms. A small zone of high compressive stress is seen in the inner flange, very close to the web. Then, a tensile stress region starts beside it and propagates toward the free edge of the flange. The transition region results in a stress concentration factor of 2 for the isotropic case and 1.5 for the orthotropic case, when compared to the maximum stress in their respective fully coiled regions. Therefore, this study has demonstrated that the stress concentration observed in the transition region is not due to material orthotropy and thus inherent to the TRAC boom itself and its coiling mechanism.



(a) Ply-2-I, integration point 1

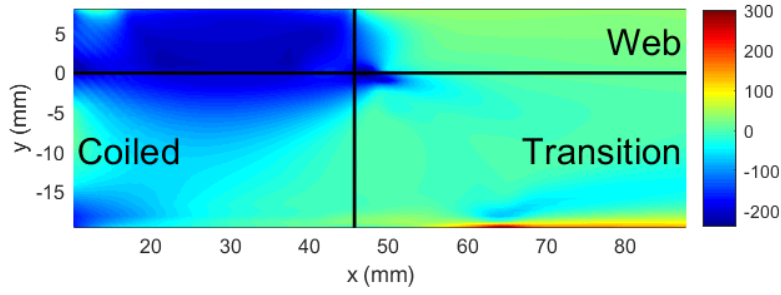


(b) Ply-2-I, integration point 2

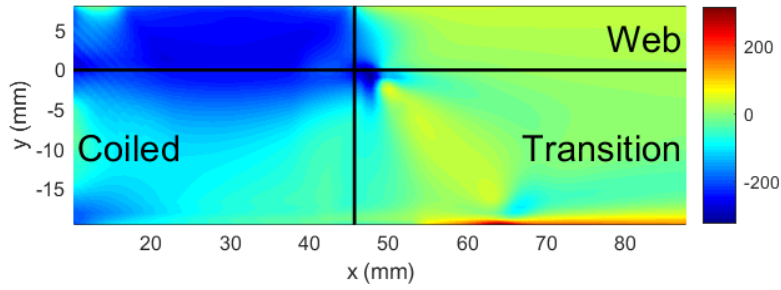


(c) Ply-2-I, integration point 3

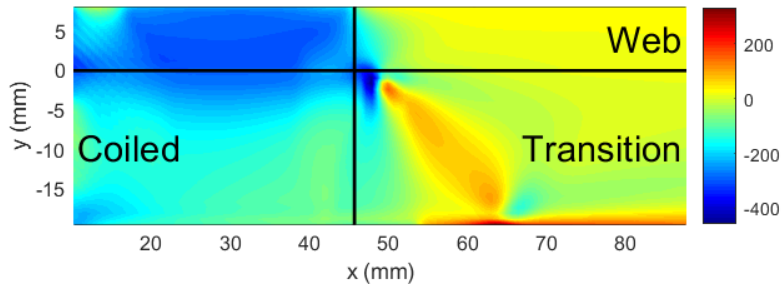
Fig. 11 σ_{xx} (MPa) in Ply-2-I of the inner flange for the reference orthotropic structure.



(a) Ply-3-I, integration point 1



(b) Ply-3-I, integration point 2



(c) Ply-3-I, integration point 3

Fig. 12 σ_{xx} (MPa) in Ply-3-I of the inner flange for the reference orthotropic structure.

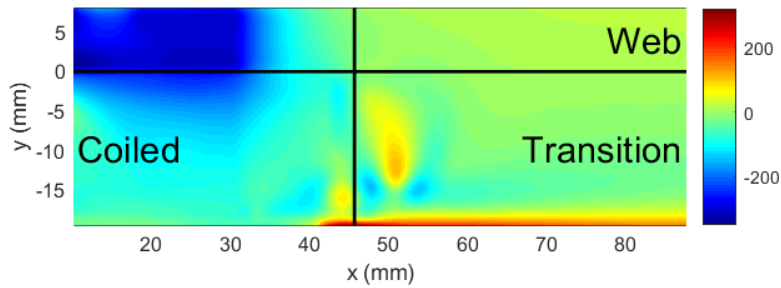


Fig. 13 σ_{xx} (MPa) in Ply-3-I, integration point 3, of the inner flange for the orthotropic boom with variable curvature cross-section.

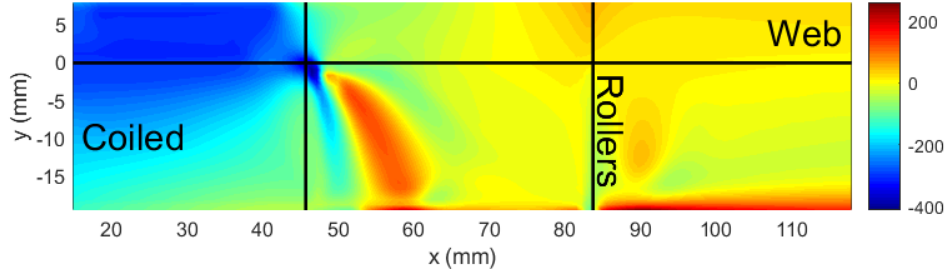


Fig. 14 σ_{xx} (MPa) in Ply-3-I, integration point 3, of the inner flange for the orthotropic boom with two-step transition region.

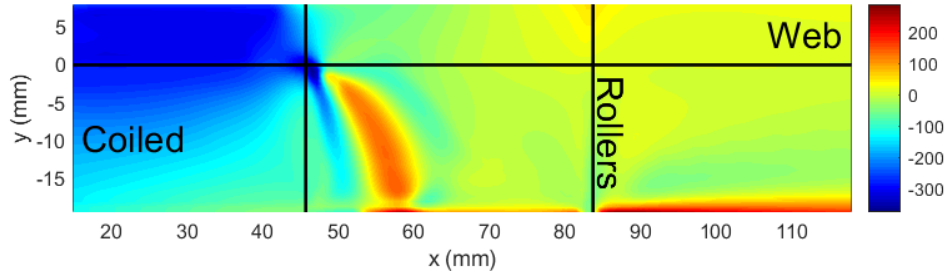


Fig. 15 σ_{xx} (MPa) in Ply-3-I, integration point 3, of the inner flange for the orthotropic boom with variable curvature cross-section and two-step transition region.

Changing the cross-section geometry was shown to reduce the maximum compressive stress by 13% and 24% for the isotropic and orthotropic booms, respectively. It is important to note that the two constraints (arc-length and opening angle) imposed on the new cross-sections greatly reduce the design space, and therefore it is likely that better performing cross-sections could be designed by relaxing one or both these two constraints. However, the present study has demonstrated that a variable curvature cross-section exhibits lower stress during coiling. Furthermore, I_{xx} and I_{yy} of the variable curvature cross-section are different from those of the reference. Hence, relaxing one or both of the constraints can also enable obtaining a required bending stiffness.

Adding nip rollers in the coiling mechanism was shown to reduce the stress concentration in the transition region by decoupling the flattening from the coiling, decreasing the stress by 26% and 11% for the isotropic and orthotropic booms respectively. Therefore, this result shows that special care must be taken when designing the boundary conditions of mechanisms for packaging and deployment of coilaible booms.

To complete the study of the orthotropic boom, a simulation integrating both the variable curvature cross-section and the new coiling mechanism was performed. The resulting longitudinal stress (for $R_N = 10$ mm and $d_N = 35$ mm) in ply-3-I, integration point 3, is shown in Figure 15. The maximum compressive stress is -380 MPa, a reduction of 17% when compared with the reference case. This maximum stress is higher than what was obtained for the variable curvature cross-section with the initial mechanism (-350 MPa). A similar study could be performed to identify a variable curvature cross-section that further reduces stress concentration given a mechanism imposing a two-step transition region.

VI. Conclusion

High stress concentration during packaging of ultra-thin coilaible structures leads to material failure when trying to wrap around hub with small diameter. Therefore, the current work investigated three methods for reducing the stress concentration factor using finite element analysis: changing the cross-section geometry, modifying the coiling mechanism, and varying the composite laminates. Booms made of isotropic material were first studied in order to decouple material properties from the effect of the cross-section geometry and the boundary conditions during coiling. Improving the cross-section and modifying the coiling process were shown to reduce stress by 13% and 26% respectively. For the orthotropic boom, a new laminate was proposed. Stress reduction of 24% and 11% were achieved by improving

the cross-section and by modifying the coiling process. Furthermore, the stress in the transition region was shown to be equal to the stress in the coiled region in the case of the variable curvature cross-section. This demonstrates that the proposed solution allows the boom composite laminate to be only limited by the stress in the coiled configuration, simplifying greatly the design process. Finally, while the current work demonstrated significant stress reduction in the booms, in future coupling of the present analysis framework with a material failure model would be important to better predict successful coiling of the proposed improved designs.

Acknowledgments

The authors acknowledge financial support from the Space Solar Power Project at Caltech, the Natural Sciences and Engineering Research Council of Canada and the Keck Institute for Space Studies.

References

- [1] Murphey, T. W., and Banik, J., “Triangular rollable and collapsible boom,” , Mar. 1 2011. US Patent 7,895,795.
- [2] Banik, J., and Ardelean, E., “Verification of a retractable solar sail in a thermal-vacuum environment,” *51st AIAA/ASME/ASCE/AHS/ASC Structures, Structural Dynamics, and Materials Conference 18th AIAA/ASME/AHS Adaptive Structures Conference 12th*, AIAA, Orlando, FL, 2010, p. 2585.
- [3] McNutt, L., Johnson, L., Clardy, D., Castillo-Rogez, J., Frick, A., and Jones, L., “Near-Earth Asteroid (NEA) Scout,” *AIAA Space 2014 Conference*, San Diego, CA, 2014.
- [4] Whorton, M., Heaton, A., Pinson, R., Laue, G., and Adams, C., “Nanosail-D: the first flight demonstration of solar sails for nanosatellites,” *22nd AIAA/USU Conference on Small Satellites*, 2008.
- [5] Johnson, L., Whorton, M., Heaton, A., Pinson, R., Laue, G., and Adams, C., “NanoSail-D: A solar sail demonstration mission,” *Acta Astronautica*, Vol. 68, No. 5, 2011, pp. 571–575.
- [6] Biddy, C., and Svitek, T., “LightSail-1 solar sail design and qualification,” *Proceedings of the 41st Aerospace Mechanisms Symposium*, Pasadena, CA, 2012.
- [7] Banik, J., and Murphey, T. W., “Performance Validation of the Triangular Rollable and Collapsible Mast,” *Proceedings of the 24th Annual AIAA/USU Conference on Small Satellites*, AIAA, Logan, UT, 2010.
- [8] Leclerc, C., Wilson, L., Bessa, M. A., and Pellegrino, S., “Characterization of Ultra-Thin Composite Triangular Rollable and Collapsible Booms,” *4th AIAA Spacecraft Structures Conference*, Grapevine, TX, 2017, p. 0172.
- [9] Murphey, T. W., Turse, D., and Adams, L., “TRAC Boom Structural Mechanics,” *4th AIAA Spacecraft Structures Conference*, Grapevine, TX, 2017.
- [10] Leclerc, C., and Pellegrino, S., “Ultra-Thin Composite Deployable Booms,” *IASS Annual Symposium “Interfaces: architecture . engineering . science”*, Hamburg, Germany, 2017.
- [11] Fernandez, J. M., “Advanced Deployable Shell-Based Composite Booms for Small Satellite Structural Applications Including Solar Sails,” *4th International Symposium on Solar Sailing*, Tokyo, Japan, 2017.
- [12] Cox, K., and Medina, K., “An Investigation of Inner Flange Buckling in Furlable Composite Booms,” *Proceedings of the American Society for Composites—Thirty-third Technical Conference*, 2018.
- [13] Leclerc, C., Pedivellano, A., and Pellegrino, S., “Stress Concentration and Material Failure During Coiling of Ultra-Thin TRAC Booms,” *2018 AIAA Spacecraft Structures Conference*, Orlando, FL, 2018, p. 0690.
- [14] Good, J. K., and Roisum, D. R., *Winding: machines, mechanics and measurements*, DEStech Publications, INC, Lancaster, PA, 2008.
- [15] Peterson, M. E., and Murphey, T. W., “Large deformation bending of thin composite tape spring laminates,” *54th AIAA/ASME/ASCE/AHS/ASC Structures, Structural Dynamics, and Materials Conference*, 2013, p. 1667.
- [16] Murphey, T. W., Francis, W., Davis, B., and Mejia-Ariza, J. M., “High strain composites,” *2nd AIAA Spacecraft Structures Conference*, 2015, p. 0942.
- [17] Roybal, F., Banik, J., and Murphey, T., “Development of an elastically deployable boom for tensioned planar structures,” *48th AIAA/ASME/ASCE/AHS/ASC Structures, Structural Dynamics, and Materials Conference*, 2007, p. 1838.